

Adaptive Local Neighborhood-based Neural Networks for MR Image Reconstruction from Undersampled Data

Shijun Liang, *Student Member, IEEE*, Anish Lahiri, *Member, IEEE*, Saiprasad Ravishankar, *Senior Member, IEEE*

Abstract—Recent medical image reconstruction techniques focus on generating high-quality medical images suitable for clinical use at the lowest possible cost and with the fewest possible adverse effects on patients. Recent works have shown significant promise for reconstructing MR images from sparsely sampled k-space data using deep learning. In this work, we propose a technique that rapidly estimates deep neural networks directly at reconstruction time by fitting them on small adaptively estimated neighborhoods of a training set. In brief, our algorithm alternates between searching for neighbors in a data set that are similar to the test reconstruction, and training a local network on these neighbors followed by updating the test reconstruction. Because our reconstruction model is learned on a dataset that is in some sense similar to the image being reconstructed rather than being fit on a large, diverse training set, it is more adaptive to new scans. It can also handle changes in training sets and flexible scan settings, while being relatively fast. Our approach, dubbed LONDN-MRI, was validated on multiple data sets using deep unrolled reconstruction networks. Reconstructions were performed at four fold and eight fold undersampling of k-space with 1D variable-density random phase-encode undersampling masks. Our results demonstrate that our proposed locally-trained method produces higher-quality reconstructions compared to models trained globally on larger datasets as well as other scan-adaptive methods.

Index Terms—Magnetic resonance imaging, machine learning, deep learning, unrolling, compressed sensing.

I. INTRODUCTION

In applications like X-ray computed tomography (CT) [1] and magnetic resonance imaging (MRI) [2], reconstructing images from undersampled or corrupted observations is of critical importance. For example, this is necessary to reduce a patient’s exposure to radiation in CT or reduce time spent acquiring MRI data. MRI scans involve sequential data acquisition resulting in long acquisition times that are not only a

© 2024 IEEE. Personal use of this material is permitted. Permission from IEEE must be obtained for all other uses, in any current or future media, including reprinting/republishing this material for advertising or promotional purposes, creating new collective works, for resale or redistribution to servers or lists, or reuse of any copyrighted component of this work in other works.

S. Liang is with the Department of Biomedical Engineering, Michigan State University, East Lansing, MI, 48824 USA (liangs16@msu.edu).

The work was done when A. Lahiri was with the Department of Electrical and Computer Engineering, University of Michigan, Ann Arbor, MI, 48901 USA (anishl@umich.edu).

S. Ravishankar is with the Department of Computational Mathematics, Science and Engineering and the Department of Biomedical Engineering, Michigan State University, East Lansing, MI, 48824 USA (ravisha3@msu.edu).

This work was supported in part by a research gift from the Advanced Radiology Services (ARS) Foundation.

burden for patients and hospitals, but also make MRI susceptible to motion artifacts. Reconstructing images from limited measurements can speed up the MRI scan, but usually entails solving an ill-posed inverse problem. Recent approaches to accelerating MRI acquisition such as compressed sensing (CS) [3] reduce scan time by collecting fewer measurements while preserving image quality by exploiting image priors or regularizers. Historically, regularization in CS-MRI has been based on sparsity of wavelet coefficients [4] or using total variation [5]. While conventional CS assumes sparsity of signals in known bases, approaches based on learned image models have been shown to be more effective for MRI reconstruction, starting with learned synthesis dictionaries [6], [7]. The dictionary parameters could be learned from unpaired clean image patches from a dataset and used for reconstruction or learned simultaneously with image reconstruction [6], [8]–[10]. Additionally, recent advances in sparsifying transform learning have resulted in efficient or inexpensive data-adaptive sparsity-based reconstruction frameworks for MRI [11]–[13]. Other contemporary techniques could allow learning explicit regularizers in a supervised manner [14] for improved image restoration.

Deep learning (DL) has emerged as a potent methodology for tackling large-scale inverse problems, notably in enhancing image reconstruction techniques in MRI and CT. Predominantly, end-to-end CNN, as exemplified by the U-net model [15], [16], have been employed to mitigate artifacts arising from undersampling in MRI data. Additionally, a plethora of alternative network models such as the Transformer [17], and Generative Adversarial Networks (GANs) [18], have demonstrated their effectiveness in MRI reconstruction, as detailed in comprehensive reviews like [12]. Furthermore, transfer learning [19] has also been used with neural networks for MRI reconstruction to achieve domain transfer.

To enhance both stability and performance, hybrid-domain approaches such as [20] enforce data consistency (i.e., the reconstruction is enforced to be consistent with the measurement model) all through training and reconstruction. Networks incorporating data consistency layers are pivotal in MR imaging for maintaining alignment between the reconstructed image and the original data in k-space [21], [22]. This category encompasses various methodologies, including deep unrolling-based methods [23], [24] (which adapt traditional iterative algorithms to learn regularization parameters), regularization by denoising approaches [25], and plug-and-play methods [26],

among others. Distinctively, the ADMM-CSNet [23] utilizes neural networks for the optimization of ADMM parameters, diverging from the ISTA-Net [27], which focuses on refining CS reconstruction models grounded in the Iterative Shrinkage-Thresholding Algorithm. The 1D deep low-rank and sparse network (ODLS) [28] demonstrates enhanced robustness for 2D MR image reconstruction, particularly in scenarios characterized by a limited number of training samples. While these deep learning-based reconstruction methods have demonstrated superiority over traditional CS techniques, concerns regarding their stability and interpretability persist, as highlighted in [29].

Apart from algorithmic advances, another driving force behind deep learning-based reconstruction is the rapid growth of publicly available training datasets. The availability of (paired or unpaired) training data sets made possible by efforts like OCMR [30] and fastMRI [31] has enabled rapidly demonstrating the capacity of deep learning-based algorithms for improved image reconstruction or denoising in MRI applications.

However, one major drawback of these learned approaches is that they typically require large training datasets such as fully sampled MRI data to be effective. A recent scan-specific deep learning method is the deep image prior [32], which has been applied to MRI [33] and learns a neural network for reconstruction in an unsupervised fashion from a single image's measurements. Other scan-adaptive methods include RAKI [34], which is a nonlinear deep learning-based autoregressive auto-calibrated reconstruction method. RAKI could be viewed as a deep neural network-based version of the parallel imaging scheme GRAPPA [35]. LORAKI [36], [37] is another scheme that trains an autocalibrated recurrent neural network (RNN) to recover missing k-space data. All these methods learn scan-specific networks without requiring large datasets. A related approach dubbed self-supervised learning has also shown promise for MRI [38] and uses a large unpaired data set.

A. Contributions

While deep learning approaches have gained popularity for MRI reconstruction due to their ability to model complex data sets, they often have difficulties generalizing to new data or distinct experimental situations at test time.

Deep CNNs usually require enormous datasets for offline training to ensure adequate performance trade-offs. In this work, we propose to learn adaptive LOcal NeighborhooD-based Networks for MRI (LONDN-MRI) reconstruction. The approach efficiently learns reconstruction networks from small clusters in a training set, directly at reconstruction time.

- The proposed models are trained using a small number of adaptively chosen neighbors that are in proximity (or are similar in a sense) to the underlying (to be reconstructed) image (cf. [39] for a slightly related approach in the context of patch-based dictionary learning).
- We show connections of this algorithm to a challenging bilevel optimization problem. Our algorithm for image reconstruction alternates between finding a small set of

similar images to a current reconstruction, training the network locally on such neighbors, and updating the reconstruction.

- The proposed local learning approach is flexible and can be seamlessly integrated with various existing deep learning frameworks for MRI, such as unrolled networks and image-domain denoisers, to enhance their performance.
- Our experimental results on multiple datasets (fastMRI, Stanford FSE, and fastMRI+) and across multiple k-space undersampling factors show that the proposed local adaptation techniques surpass networks trained globally on larger datasets. We demonstrate improved performance against scan-specific deep learning methods such as deep image prior, RAKI, and LORAKI, even when using a small number of neighbors for training.
- We have shown the method's generalizability under different scenarios including different sampling patterns, and testing on data with artificial as well as natural lesions, when the training dataset didn't include such lesions. To establish clinical utility, we also conducted tests under different MR scan contrast settings and varying signal-to-noise ratios at test time, where the proposed method showed promise. Our study also encompassed an analysis of image quality vs. time consumption trade-offs when involving different networks and number of neighbors selected, and compared favorably with related approaches.

B. Organization

The rest of this article is organized as follows. Section II discusses some preliminaries on multi-coil MRI reconstruction and the approach for searching neighbors that will be used in our algorithm. Section III describes the proposed technique and its interpretations. Section IV presents the experimental setup and results. Section V provides a discussion of our findings, and in Section VI, we conclude.

II. PRELIMINARIES

A. Multi-coil MRI Reconstruction

When an image $\mathbf{x} \in \mathbb{C}^q$ (vectorized) is sufficiently sparse in some transform domain and the transform is sufficiently incoherent with the measurement operator, compressed sensing theory [3], [40] enables accurate image recovery from limited measurements. The image reconstruction problem in MRI is typically formulated as an optimization of a data-fidelity penalty and a regularizer as follows:

$$\hat{\mathbf{x}} = \arg \min_{\mathbf{x}} \sum_{c=1}^{N_c} \|\mathbf{A}_c \mathbf{x} - \mathbf{y}_c\|_2^2 + \lambda \mathcal{R}(\mathbf{x}), \quad (1)$$

where $\mathbf{y}_c \in \mathbb{C}^p$, $c = 1, \dots, N_c$, represent the acquired k-space measurements from N_c coils. We write the imaging forward operator or measurement operator as $\mathbf{A}_c = \mathbf{M} \mathcal{F} \mathbf{S}_c$, where $\mathbf{M} \in \{0, 1\}^{p \times q}$ is a masking operator that captures the undersampling pattern in k-space, $\mathcal{F} \in \mathbb{C}^{q \times q}$ is the Fourier transform operator (corresponding to densely sampled measurements), and $\mathbf{S}_c \in \mathbb{C}^{q \times q}$ is the c th coil-sensitivity matrix (a diagonal matrix). Additionally, the regularizer above

may include a slew of terms capturing the assumed model of the underlying image. It enables enforcing desirable properties such as spatial smoothness, image sparsity, or edge preservation in the reconstructed image. Numerous iterative optimization techniques exist for (1).

In MRI, the regularizer can involve ℓ_1 penalty on wavelet coefficients [4] or a total variation penalty [5] or patch-based sparsity in learned dictionaries [6] or sparsifying transforms [13], or proximity to deep learning-based reconstructions, etc. For example, sparsity w.r.t. a known transform matrix \mathbf{W} is captured by $\mathcal{R}(\mathbf{x}) = \|\mathbf{W}\mathbf{x}\|_1$.

B. Neighbor Search

Our approach relies on finding images in a data set that are in a sense similar to the one being reconstructed. The similarity may be defined using a metric such as Euclidean distance or other metrics. Assume we have a data set $\{\mathbf{x}_n, \mathbf{y}_n\}_{n=1}^N$ with N reference or ground-truth images \mathbf{x}_n and their corresponding k-space measurements \mathbf{y}_n (with multi-coil data), we use the distance metric d to find the k nearest neighbors to an (estimated/reconstructed) image \mathbf{x} as follows:

$$\hat{C}_{\mathbf{x}} = \arg \min_{C \in \mathcal{C}, |C|=k} \sum_{r \in C} d(\mathbf{x}, \mathbf{x}_n), \quad (2)$$

where C is a set of cardinality k containing indices of feasible neighbors, and \mathcal{C} denotes the set of all such sets with k elements. Different distance functions could produce a different set of similar neighbors, which could then affect the outcome of the reconstruction algorithm, as our network modeling is dependent on the choice of the local data set.

As a result, we used different metrics for evaluating our approach in this work. The distances serve as a proxy for data similarity, with nearby data considered similar and distant data considered dissimilar. We used the Manhattan distance, Euclidean distance, and normalized cross-correlation as distance metrics as follows.

$$\begin{aligned} d^{L1}(\mathbf{x}, \mathbf{x}_n) &= \|\mathbf{x} - \mathbf{x}_n\|_1 \\ d^{L2}(\mathbf{x}, \mathbf{x}_n) &= \|\mathbf{x} - \mathbf{x}_n\|_2 \\ d^{NCC}(\mathbf{x}, \mathbf{x}_n) &= 1 - \frac{|\mathbf{x}^H \mathbf{x}_n|}{\|\mathbf{x}\|_2 \|\mathbf{x}_n\|_2}. \end{aligned}$$

In all cases, we select the top k most similar neighbors (from a set) that correspond to the k smallest distances in (2). The indices of the chosen images are in the set $\hat{C}_{\mathbf{x}}$, i.e., they are the minimizer in (2). These neighbors can be used to train the local model. These are expected to capture structures most similar to the image being reconstructed, enabling a highly effective reconstruction model to be learned.

III. PROPOSED LONDN-MRI ALGORITHM

Our primary objective is to learn an adaptive neural network for MRI reconstruction, in which the model's free parameters are fitted using training data that are similar in a sense to the current scan. We emphasize that the proposed model is local in the sense that it changes in response to the input. The advantage of the proposed method is that the model is fit

for every scan and can thus be adaptive to the scan, readily handling changes in sampling masks, for example.

The algorithm begins by obtaining an initial estimate of the underlying image, denoted \mathbf{x}^0 , from undersampled measurements \mathbf{y} . Our proposed strategy then alternates between computing the closest neighbors to the reconstruction in the training set and performing CNN-based supervised learning on the estimated local dataset. During supervised learning, the network weights could be randomly initialized or could be warm started with the weights of a pre-trained (e.g., state-of-the-art) network. In the latter case, the pre-trained network would adapt to the features of images similar to the one being reconstructed (akin to transfer learning [19]).

In each iteration, the nearest ground truth images in the training set are computed in relation to the reconstruction (estimate) predicted by the locally learned network, except in the first iteration, when the nearest neighbors are computed in relation to the (typically highly aliased) initial \mathbf{x}^0 (we used corresponding aliased images in the dataset for computing distances in the first iteration). In practice, pairwise distances to even a large number of images can be computed very efficiently (in parallel), after which the local network can be rapidly learned on a small set of neighbors (typically a shallow network or with early stopping). The network weights for deep reconstruction are constantly updated to map the initial images for the local data set to the target (ground truth) versions.

To demonstrate our approach, we used the state-of-the-art deep CNN reconstruction model MoDL [20], which is trained locally in our scheme. Additionally, we trained it globally, i.e., once on a larger dataset, in order to compare it to our on-the-fly neighborhood-based learning scheme. For completeness, we briefly recap the MoDL scheme in the following and discuss its local training within our framework. MoDL is similar to the plug-and-play approach, except that instead of pre-trained denoiser networks, end-to-end training is used to learn the shared network weights across iterations in the architecture.

A. Network Model and Training

The proposed approach is compatible with any network architecture. We use MoDL, which has shown promise for MR image reconstruction, and combines a denoising network with a data consistency (DC) module in each iteration of an unrolled architecture. MoDL unrolls alternating minimization for the following problem:

$$L_a(\mathbf{z}, \mathbf{x}) := \nu \sum_{c=1}^{N_c} \|\mathbf{A}_c \mathbf{x} - \mathbf{y}_c\|_2^2 + \mathcal{R}(\mathbf{z}) + \mu \|\mathbf{x} - \mathbf{z}\|_2^2. \quad (3)$$

We denote the initial image in the process as \mathbf{x}^0 , $\nu \geq 0$ weights the data-consistency term above, and $\mu \geq 0$ weights the proximity of \mathbf{x} to \mathbf{z} . By decomposing the optimization into two subproblems over \mathbf{z} and \mathbf{x} , the explicit regularizer-based update for \mathbf{z} can be solved by replacing it with a CNN-based denoiser ($D_\theta(\cdot)$), and the denoised estimate is then used to update \mathbf{x} . The \mathbf{x} update in the MoDL scheme involves the data-consistency term and is performed using Conjugate Gradient (CG) descent. Thus, \mathbf{z} is obtained as the output from a CNN-based denoiser (D_θ) and \mathbf{x} is updated by CG.

This alternating scheme is repeated L times (unrolling), with the initial input image \mathbf{x}^0 being passed through L blocks of denoising CNN + CG updates. Now, if $\mathbf{S}_\theta^l(\cdot)$ is the function capturing the l th iteration of the algorithm, then the MoDL output for the l th block is given as

$$\begin{aligned} \mathbf{x}^{l+1} &= \mathbf{S}_\theta^l(\mathbf{x}^l) = \mathbf{S}(\mathbf{x}^l, \theta, \nu_l, \{\mathbf{A}_c, \mathbf{y}_c\}_{c=1}^{N_c}), \text{ and} \\ \mathbf{S}(\bar{\mathbf{x}}, \theta, \nu, \{\mathbf{A}_c, \mathbf{y}_c\}_{c=1}^{N_c}) &\triangleq \\ \arg \min_{\mathbf{x}} \nu \sum_{c=1}^{N_c} &\|\mathbf{A}_c \mathbf{x} - \mathbf{y}_c\|_2^2 + \|\mathbf{x} - \mathbf{D}_\theta(\bar{\mathbf{x}})\|_2^2. \end{aligned} \quad (4)$$

After L iterations, the final output is

$$\mathbf{x}_{\text{supervised}} = \mathbf{x}^L = \left(\bigcirc_{l=0}^{L-1} \mathbf{S}_\theta^l \right) (\mathbf{x}^0) \triangleq \mathbf{M}_\theta(\mathbf{x}^0), \quad (5)$$

where \mathbf{M}_θ denotes the end-to-end mapping, $\bigcirc_{l=0}^{L-1} f^i$ represents the composition of L functions $f^{L-1} \circ f^{L-2} \circ \dots \circ f^0$, and \mathbf{x}^0 is the initial image. The weights of the denoiser \mathbf{D}_θ are shared across the L blocks. The network parameters θ are learned in a supervised manner so that $\mathbf{x}_{\text{supervised}}$ matches known ground truths (in mean squared error or other metric) on a (large/global or local) training set. This involves the following optimization for training:

$$\begin{aligned} \hat{\theta} &= \arg \min_{\theta} \sum_{n \in S} C_\beta(\mathbf{M}_\theta(\mathbf{x}_n^0); \mathbf{x}_n) \\ &= \arg \min_{\theta} \sum_{n \in S} (\|\mathbf{x}_n - \mathbf{M}_\theta(\mathbf{x}_n^0)\|_2^2), \end{aligned}$$

where n indexes the samples from the data set used for training, with \mathbf{x}_n denoting the n th target (or ground truth) image reconstructed from fully-sampled k-space measurements and \mathbf{x}_n^0 denotes the initial image estimate from undersampled measurements. The cost $C_\beta(\hat{\mathbf{x}}_n; \mathbf{x}_n)$ denotes the training loss. The main difference between a globally learned and locally learned network is the choice of the set S of training indices. For the proposed local approach, we fit the network based on the k training samples closest to the current test image estimate, whereas the conventional (or global) training would fit networks to a large dataset. The initial image estimate \mathbf{x}_n^0 is obtained from the undersampled measurements \mathbf{y}_n using a simple analytical reconstruction scheme such as applying the adjoint of the forward model to the measurements.

In each iteration, the network is updated (Fig. 1), and the initial estimate of the underlying unknown image is passed through the network to obtain a new estimate. In Fig. 1, we illustrate the iterative process of neighbor fine-tuning and local network updating. Local learning may have the advantage of accommodating changes in experimental conditions (e.g., undersampling pattern) at test time, provided that such modified measurements and initial images for the small local training set can be easily simulated from the existing \mathbf{x}_n or \mathbf{y}_n . Our overall algorithm is also summarized in Algorithm 1.

B. Regularization

In order to avoid over-fitting when training networks on small sets, we also adopted regularization of weights during

Algorithm 1 LONDN-MRI Algorithm

Require: Initial image \mathbf{x}^0 , number of neighbors k , k-space undersampling mask \mathbf{M} , regularization parameters ν and μ , number of training epochs T , number of iterations of alternating algorithm S .

- 1: Initialize reconstruction network parameters θ with pre-learned network weights $\hat{\theta}$ or randomly initialized weights. Set $\mathbf{x} = \mathbf{x}^0$.
- 2: **for** Iteration $<$ maximal iteration S **do**
- 3: Compute the set of k similar neighbors $\hat{C}_\mathbf{x}$ to the current reconstruction estimate \mathbf{x} using metric d .
- 4: **for** epoch $<$ maximal number T **do**
- 5: For each batch of neighbor data, compute the gradient of the training loss with respect to the network parameters θ and perform one update step on θ .
- 6: **end for**
- 7: Update $\mathbf{x} \leftarrow \mathbf{M}_\theta(\mathbf{x}^0)$
- 8: **end for**
- 9: **return** reconstruction \mathbf{x} and learned net. parameters θ .

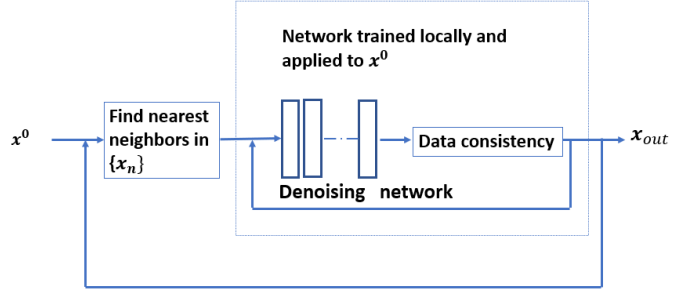


Fig. 1: Flowchart of the proposed LONDN-MRI scheme with a specific unrolled reconstruction network. The denoising network could be for example a U-Net or the recent DIDN.

training as follows:

$$\hat{\theta} = \arg \min_{\theta} \sum_{n \in S} \|\mathbf{x}_n - \mathbf{M}_\theta(\mathbf{x}_n^0)\|_2^2 + \lambda \mathcal{R}(\theta), \quad (6)$$

where $\mathcal{R}(\cdot)$ denotes the regularization term on network weights. We primarily used the ℓ_1 norm regularizer to enforce sparsity of the network weights to learn simpler models. We observed that regularizing the local model enables it to converge more easily, and shrinks weights for less important or noisy features to zero. We provide more discussion in the experiments section.

C. Connections to Bilevel Optimization

The alternating algorithm for training involving a neighbor search step and a local network update step could be viewed as a heuristic algorithm for the following bilevel optimization

problem:

$$\begin{aligned} & \min_{C \in \mathcal{C}, |C|=k} \sum_{i \in C} \|f_{\theta(C)}(\mathbf{y}) - \mathbf{x}_i\|_2^2, \\ \text{s.t. } & \theta(C) = \arg \min_{\theta} \sum_{i \in C} \|\mathbf{x}_i - f_{\theta}(\mathbf{y}_i)\|_2^2. \end{aligned} \quad (7)$$

Here, $f_{\theta(C)}$ denotes a deep neural network learned on a subset C of a data set that maps the current k-space measurements \mathbf{y} to a reconstruction. The network is akin to $\mathcal{M}_{\theta}(\mathbf{x}^0)$ shown earlier (6), but with \mathbf{x}^0 assumed to be generated from \mathbf{y} (e.g., via the well-known sum of squares of coil-wise inverse Fourier transforms, or via SENSE reconstruction, etc.). Problem 7 aims to find the best neighborhood or cluster among the training data, where the reconstructed image belongs (with closest distances to neighbors – we assumed Euclidean distance here), with the network weights for reconstruction estimated on the data in that cluster. Problem 7 is a bilevel optimization problem with the cluster optimization forming the upper level cost and network optimization forming the lower level cost. Bilevel problems are known to be quite challenging [14], [41]. It is also a combinatorial problem because we would have to sweep through all possible choices of clusters of k training samples with reconstruction networks trained in each such cluster, to determine the best cluster choice.

The proposed algorithm is akin to optimizing the bilevel problem by optimizing for the network weights θ with the clustering C fixed (the lower level problem) and then optimizing for the clustering C (upper level minimization) with the network weights fixed. This is a heuristic because the optimized variables in each step are related, however, such an approach has been used in prior work [10] and shown to be approximately empirically convergent for the bilevel cost. In this work, we performed an empirical evaluation of convergence in the experiments section, where the alternating algorithm is shown to reduce the upper-level cost in (7).

IV. EXPERIMENTS

We first present the overall experimental setup in Section IV-A. Key results and comparisons are presented in Section IV-B. The intricacies and behavior of LONDN-MRI are analyzed in Section IV-C and its generalizability is investigated in Section IV-D.

A. Experimental Setup

Datasets & Models: We evaluated the effectiveness of the proposed LONDN-MRI reconstruction method on multiple datasets: the multi-coil fastMRI knee and brain datasets [31], [42], the fastMRI+ dataset¹ (which is just an annotated version of fastMRI indicating pathologies), and the Stanford 2D FSE [43] dataset. The results obtained on the fastMRI knee dataset and the Stanford FSE data are described in Section IV-B. The fastMRI brain and fastMRI+ data are used in the studies in Section IV-D. For training, we randomly selected a subset of 3000 images from the fastMRI knee and brain datasets and the same for the fastMRI+ case. We used

2000 training images for the smaller Stanford FSE dataset. We used 15 or 20 images for testing in different scenarios, which were randomly chosen. In some experiments, we evaluated the effect of training set size, where we worked with fewer or more images in the training set.

Coil sensitivity maps for model-based reconstruction were generated for each scan using the BART toolbox [44]. We tested obtaining these using either the fully-sampled k-space or only center of k-space data and noticed very little difference in reconstruction quality between the two approaches.

Since the proposed LONDN-MRI framework is quite general and can be combined with any supervised deep learning based reconstruction approach, we chose the recent popular model-based deep learning (MoDL) reconstruction network and compared globally (over large set of training samples) and locally (over very small matched set of samples) learned versions of the model for different choices of deep denoisers in the network². We performed reconstructions at fourfold or 4x acceleration (25.0% sampling) as well as at eightfold or 8x acceleration (12.5% sampling) of the k-space acquisition. In all cases, variable density 1D random Cartesian (phase-encode) undersampling of k-space was performed. The initial image estimates for MoDL were obtained by applying the adjoint of the measurement operator to the subsampled k-space data, and were then used to train both local and global versions of MoDL networks. In our local versions (LONDN-MRI), we used 30 images for training (searched from e.g., 3000 images), while the global versions used the full subset of training images.

Network Architectures & Training: We trained two types of MoDL models at 4x and 8x k-space undersampling, respectively. One used the well-known UNet denoiser, with a two-channel input and two-channel output, where the real and imaginary parts of an image are separated into two channels. The network weights during training were initialized randomly (normally distributed). The ADAM optimizer was utilized for training the network weights. For LONDN-MRI, we used an initial learning rate of 6×10^{-5} with a multi-step learning rate scheduler, which decreases the learning rate at 100 and 150 epochs with learning rate decay 0.65. For training globally, we used an initial learning rate of 1×10^{-4} with 150 epochs of training and a multi-step learning rate scheduler that decreased the learning rate at 50 and 100 epochs with learning rate decay 0.6. For LONDN-MRI, MoDL with 5 iterations was used with a shallow UNet that had 2 layers in the encoder and decoder, respectively. We used a shallow network with dropout for the local model to avoid over-fitting to the very small training set.

For the MoDL network trained globally (on large dataset) for making comparisons with, we utilized 4 layers in the decoder and encoder in UNet and 6 MoDL blocks. We used a batch size of 2 during training for both the global and local cases. Furthermore, for the data-consistency term, we used a tolerance of 10^{-5} in CG and a μ/ν ratio of 0.1. Also, we chose the regularization weight λ as 10^{-9} for LONDN-MRI, unless specified otherwise.

²See https://github.com/sjames40/Multi_coil_local_model for our code in PyTorch.

¹<https://github.com/microsoft/fastmri-plus/tree/main>

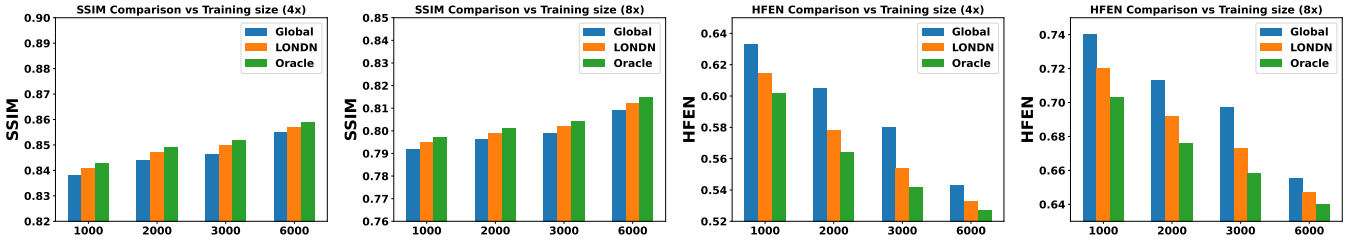


Fig. 2: Comparison of MoDL with UNet denoiser trained globally vs. using the proposed LONDNN-MRI scheme (1 iteration). Reconstruction metrics are shown across training set sizes at 4x and 8x undersampling.

For the second MoDL architecture, we used the recent state-of-the-art denoising network DIDN [45], [46]. Due to the high complexity of the DIDN network, we first pre-trained it on the larger (global) dataset (learning rate, etc., similar to the UNet case) before adapting the weights within LONDNN-MRI for each scan. This is an alternative to constructing shallower versions of a network for local adaptation.

The ADAM optimizer was utilized for training, with a learning rate of 5×10^{-5} in LONDNN-MRI. We used 6 iterations of MoDL with the DIDN denoiser for which we used 3 down-up blocks (DUBs). The number of epochs for training was 30 in LONDNN-MRI. The remaining training parameters were chosen similarly as in the previous UNet-based case. Using a pre-trained state-of-the-art denoiser allows the local adaptation to converge faster.

Comparison to Scan-adaptive Methods: We compared the performance of our schemes to recent related scan-specific methods such as deep image prior (DIP) [33] (using the public package³ but additionally incorporating coil sensitivity maps), RAKI [34] (using publicly available code⁴), SOUP-DIL [8] (code extracted from publicly available package⁵), and LORAKI [36] (modified from RAKI code). In our experiments, we used parameters specified in the authors' original implementations, which we observed worked well.

Sampling Masks & Performance Metrics: We used binary masks for fourfold and eightfold Cartesian undersampling of k-space. Fig. 3 shows the sampling masks primarily used in our experiments that include a fully-sampled central region (with 31 central lines at 4x acceleration and 15 central lines at 8x acceleration) and the remaining phase encode lines were sampled uniformly at random.

For the performance metrics, we used three common metrics to quantify the reconstruction quality of different methods. These were the peak signal-to-noise ratio (PSNR) in decibels (dB), structural similarity index (SSIM) [47], and the high frequency error norm (HFEN) [6], which were computed between the reconstruction and the ground truth obtained from fully-sampled k-space data. The HFEN was computed from the ℓ_2 norm of the difference between Laplacian of Gaussian (LoG) filtered reconstructed and ground truth images. This was normalized by the ℓ_2 norm of the LoG filtered ground truth.

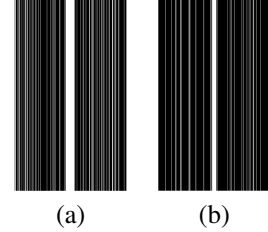


Fig. 3: Undersampling masks used in our experiments: (a) fourfold undersampled 1D Cartesian phase-encoded; and (b) eightfold undersampled 1D Cartesian phase-encoded. The masks were zero-padded for slightly larger images.

B. Results and Comparisons

Results for the UNet-based Reconstructor: Table I compares the average PSNR values for reconstruction over the fastMRI knee testing set at both 4x and 8x undersampling. We varied the number of images in the training set for a more comprehensive study. We compare learning networks over a small set of similar images to learning networks over the larger datasets (global), as well as to an oracle LONDNN scheme, where the neighbors in the training set were computed based on each ground truth test image. The oracle scheme would ideally provide an upper bound on the performance of the iterative LONDNN-MRI scheme. Moreover, LONDNN-MRI outperforms DIP, RAKI, SOUP-DIL, and LORAKI with U-Net (Table I). Note that DIP, RAKI, SOUP-DIL, and LORAKI do not use information beyond the test scan (scan-adaptive). Later, we show how LONDNN-MRI performs when the overall dataset it uses is very limited.

When varying the size of the training set, the global approach was trained on the full set each time, whereas the local approach performed training on small subsets of 30 training pairs selected from the larger datasets. The iterations of the LONDNN-MRI scheme quickly improve reconstruction performance, and even with only 2 LONDNN-MRI alternations, the PSNR values begin approaching the oracle setting. The LONDNN schemes (oracle or iterative) consistently outperform the globally trained networks across the different training set sizes considered. We note that the results for the globally trained model with many (6000) training scans match closely the LONDNN-MRI results, when LONDNN-MRI uses a smaller overall training set (3000 scans) for neighbor search. This illustrates the potential of our approach with limited training

³<https://github.com/MLI-lab/ConvDecoder>

⁴<https://github.com/geop1/DeepMRI>

⁵<https://github.com/JeffFessler/BLIPSrecon/>

data, when compared with models trained on larger sets.

Figure 2 compares the SSIM and HFEN reconstruction metrics using bar graphs, where a similar trend is observed as with PSNR.

Figs. 4 and 5 show images reconstructed by different methods at 8x and 4x undersampling, respectively.

The LONDN-MRI reconstructions (either iterative or oracle) show fewer artifacts, sharper features, and fewer errors than the global MoDL and initial aliased reconstructions. The iterative LONDN-MRI results are also quite close to the oracle result.

Ax	Data size	Global	LONDN-MRI (1 iteration)	LONDN-MRI (2 iterations)	Oracle	DIP	RAKI	LORAKI	SOUPI DIL
4x	1000	32.63	32.78	32.87	32.99				
	2000	33.00	33.28	33.31	33.35	30.1	30.25	31.35	30.97
	3000	33.17	33.46	33.51	33.54				
	6000	33.48	33.58	33.65	33.69				
8x	1000	29.78	30.15	30.26	30.34				
	2000	30.21	30.53	30.58	30.64	28.9	29.01	29.71	29.47
	3000	30.47	30.76	30.80	30.85				
	6000	30.78	30.94	31.04	31.09				

TABLE I: Average reconstruction PSNRs (in dB) for 15 images at 4x and 8x k-space undersampling. The proposed LONDN-MRI (with 1 or 2 alternations) is compared to training a global reconstructor for different training set sizes and another scan based method. We also compare to an oracle local reconstructor, where neighbors are found with respect to known ground truth test images.

Results for the DIDN-based Reconstructor: To demonstrate adaptability to different network architectures, Table II compares reconstruction performance on the test set with the DIDN denoiser-based MoDL architecture. Average PSNR values with LONDN-MRI are compared to those with networks trained globally at different training set sizes. We ran only 1 iteration of LONDN-MRI, where the reconstruction with a pre-trained (global) network was used to find neighbors. PSNR values for the oracle LONDN-MRI reconstructor are also shown. The overall performances with the DIDN-based architectures are better than with the UNet-based unrolled networks. The PSNRs for LONDN-MRI are consistently and similarly better than for the globally trained network across the different training set sizes considered, indicating potential for LONDN-MRI in improving state-of-the-art models. Fig. 6 visually compares reconstructions and reconstruction errors (in zoomed in region) for different methods. We can see that the LONDN reconstructors capture the original image features more sharply and accurately than the globally learned reconstruction.

Performance on the Stanford FSE Dataset: We also performed image reconstructions with the Stanford multi-coil FSE dataset, which is a smaller dataset. We used same settings for the networks and training as in Section IV-A. Table III shows that LONDN-MRI significantly outperforms the globally learned MoDL network at both 4x and 8x acceleration. This indicates benefits for the proposed framework for smaller, more diverse datasets. Figs. 7 and 8 display visual comparisons that show the LONDN-MRI scheme recovering sharper features than the globally learned network.

Acceleration	Data Size	Global	LONDN-MRI (1 iteration)	Oracle
4x	1000	33.66	33.92	33.96
	2000	34.01	34.23	34.31
	3000	34.15	34.39	34.42
8x	1000	31.02	31.33	31.37
	2000	31.34	31.64	31.68
	3000	31.79	32.08	32.12

TABLE II: Average reconstruction PSNR values (in dB) on the testing set at 4x and 8x undersampling for various training set sizes. MoDL reconstructor with DIDN denoiser is used.

Acceleration	Global	LONDN-MRI (1 iteration)	LONDN-MRI (2 iterations)	Oracle
4x	29.45	31.49	31.56	31.67
8x	27.25	29.35	29.43	29.60

TABLE III: Average reconstruction PSNR values (in dB) for the Stanford FSE test set at 4x and 8x undersampling. The LONDN-MRI results are compared to a model globally trained on the FSE dataset.

C. Behavior of LONDN-MRI

Here, we explore the intricacies and workings of LONDN-MRI in more detail.

Performance with Different Distance Metrics: To determine a suitable distance metric for our method, we analyzed a few popular distance metrics. This study focused on evaluating their effectiveness in selecting the appropriate matching dataset for training in the context of LONDN-MRI (oracle scheme). We tested the performance of MoDL with UNet denoiser using L1 and L2 distance metrics as well as normalized cross-correlation (NCC), to find the matched training set from among 3000 images, which were all normalized. From the results in Table IV, we see that the different distance functions offer only slight differences in reconstruction performance, with NCC offering the best results with respect to all reconstruction metrics.

Acceleration	Reconstruction Metric	L1	L2	NCC
		SSIM	0.85	0.849
4x	PSNR (dB)	33.49	33.44	33.54
	HFEN	0.552	0.56	0.542
	SSIM	0.803	0.802	0.804
8x	PSNR (dB)	30.79	30.71	30.85
	HFEN	0.664	0.674	0.658
	SSIM	0.803	0.802	0.804

TABLE IV: Average PSNR, SSIM, and HFEN values over 15 testing images for LONDN-MRI with neighbor search performed using L1 distance, L2 distance, and normalized cross-correlation (NCC).

Evaluating the Accuracy of Neighbor Search: Here, we study how the neighbor search proceeds across the iterations or alternations of LONDN-MRI. We are interested to know if our locally learned reconstructor can improve the neighbor finding process over iterations. We used all images from the test set. First, we find the k closest neighbors (in terms of Euclidean distance) for each ground truth test image amongst the ground truth training images. The set C_r^* contains the

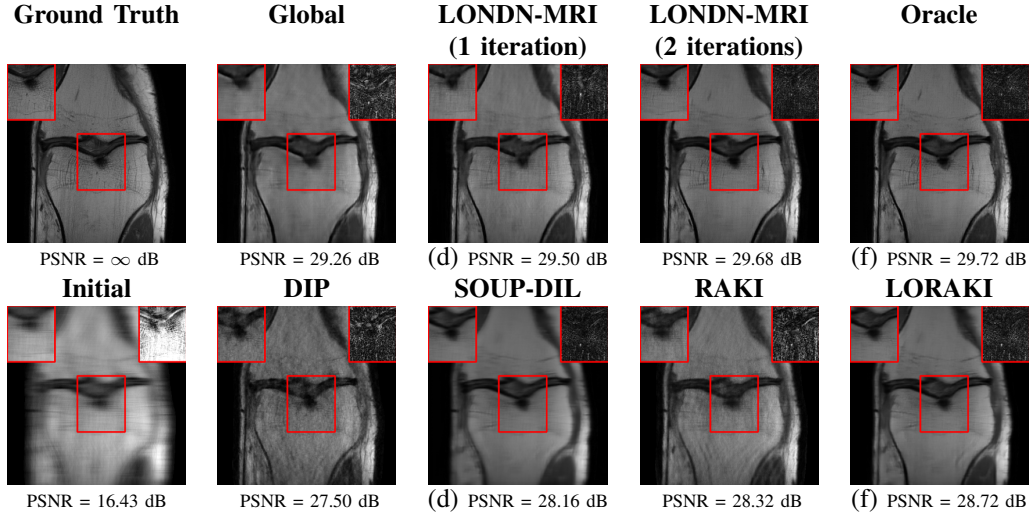


Fig. 4: Comparison of image reconstructions with different methods at 8x undersampling. The global and LONDN-MRI methods use the MoDL architecture with UNet denoiser with 1000 training images. The inset panel on the top left in each image corresponds to a section of interest in the image (shown by the red bounding box), while the inset panel on the top right corresponds to the error map with respect to the ground truth.

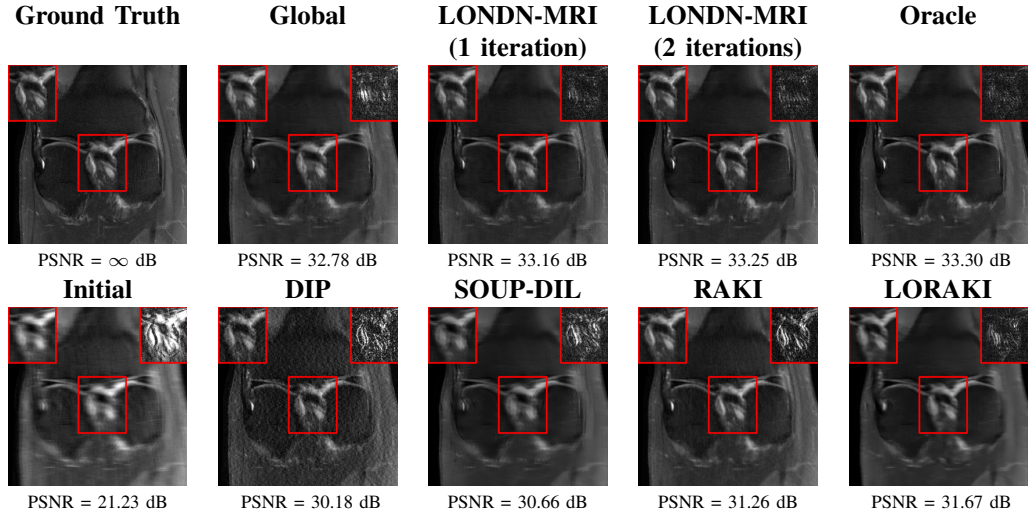


Fig. 5: Same comparisons/setup as Fig. 4, but at 4x undersampling. The supervised methods used MoDL architecture with UNet denoiser (3000 training images).

indices of these *oracle* neighbors for a test image indexed r . The set \hat{C}_r contains the indices of closest neighbors from a certain iteration of LONDN-MRI. The neighbor matching accuracy (NMA) metric below computes the average (over the test set indices \mathcal{T}) percentage match between the two sets:

$$\text{NMA} := \frac{100}{|\mathcal{T}|} \sum_{r \in \mathcal{T}} \frac{|\hat{C}_r \cap C_r^*|}{k}, \quad (8)$$

The accuracy of the neighbor search at both 4x and 8x undersampling is shown in Fig. 9. The accuracy of the initial search (based on \mathbf{x}^0) and after 1 or 2 iterations of LONDN-MRI are shown. We find nearest neighbors for the initial highly aliased \mathbf{x}^0 with respect to the corresponding aliased images in the training set (based on the same k-space undersampling mask as at testing time), rather than based on the ground truth

training images, because the latter resulted in lower neighbor search accuracy for \mathbf{x}^0 . It is clear from Fig. 9 that the accuracy improves quickly and tapers off in few iterations.

Effect of Weight Regularization in LONDN-MRI: Here, we vary the strength of the regularization penalty weight in (6) and run LONDN-MRI over the test set at 4x k-space undersampling. Fig. 10 plots the average PSNR as a function of the penalty weight for the MoDL network with UNet denoiser. The normalized cross-correlation distance was used during neighbor search, with other parameters as before. The result shows slight benefits for choosing the regularization weight carefully.

Convergence of Loss in Bilevel Optimization: Next, we study the behavior of the alternating LONDN-MRI algorithm as a heuristic for the bilevel optimization formulation in (7).

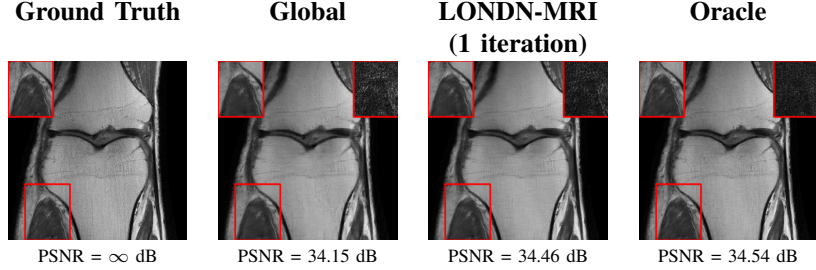


Fig. 6: Comparison of image reconstructions at 4x undersampling for the MoDL network with DIDN denoiser and 3000 training images, when compared to LONDN-MRI. A region of interest and its error are also shown.

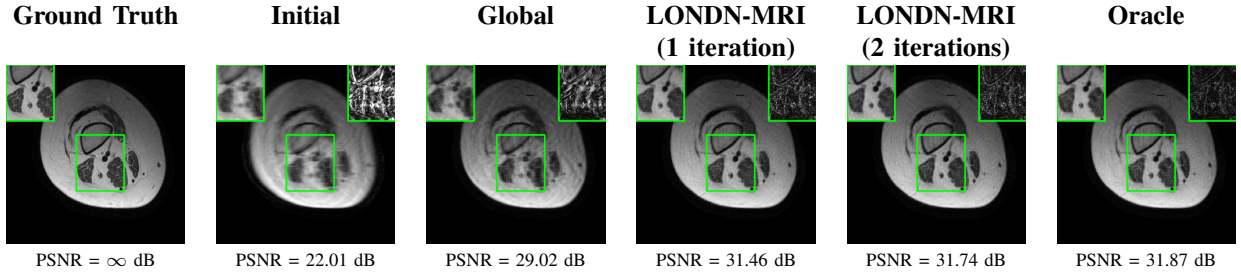


Fig. 7: Comparison of image reconstructions with different methods at 4x undersampling using MoDL architecture with UNet denoiser with 2000 training scans. The test slice and training data were from the Stanford FSE dataset.

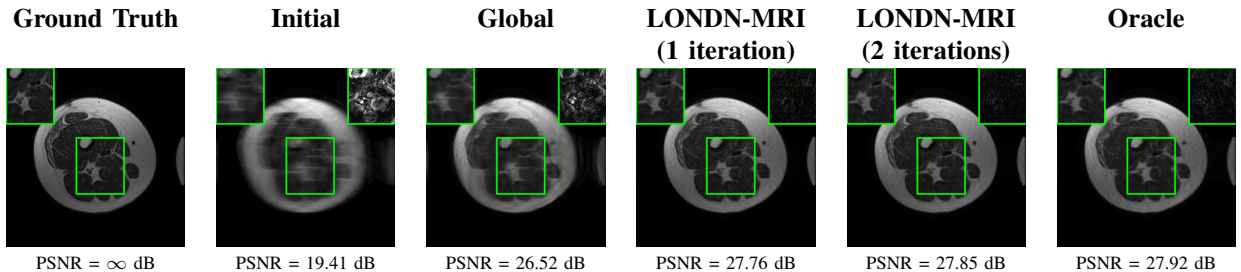


Fig. 8: Same comparisons/setup as Fig. 7, but at 8x undersampling.

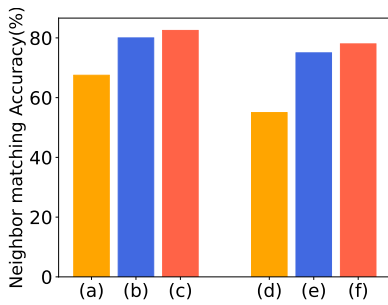


Fig. 9: Average accuracy (over test set) of neighbor search in LONDN-MRI (MoDL with UNet denoiser) at 4x undersampling in (a) the first iteration (neighbors found with respect to the initial input images x^0) and after the (b) first and (c) second iteration. (d)-(f) are corresponding results at 8x undersampling.

Here, we used an MoDL network with the UNet denoiser and $k = 30$ training pairs were chosen (from 3000 cases) in the local dataset in each iteration of LONDN-MRI. The UNet weights were randomly initialized to begin with, and the neighbor search in the first iteration of LONDN-MRI was

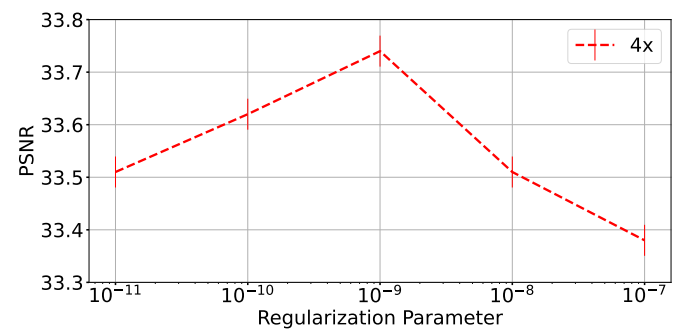


Fig. 10: Average reconstruction PSNR on the test set at 4x undersampling for different regularization penalty parameters. We used ℓ_1 norm regularization of network weights for an MoDL network with UNet denoiser.

performed using x^0 and correspondingly generated aliased training images. Fig. 11 plots the upper-level loss in (7) (in a root mean squared error form) after each iteration of LONDN-MRI for a test image. Here, we ran many iterations to verify

convergence. We observe that the loss changes very little after a few iterations and stabilizes. This matches with the behavior of the neighbor search accuracy bar plots. The result indicates that the proposed alternating scheme could be a reasonable heuristic for reducing the loss in the challenging problem (7). Finally, we compare the loss values in Fig. 11 with an oracle loss, where the upper-level loss in (7) is computed using the ground truth test image and its k nearest neighbors. The loss values in LONDN-MRI converge very close to the oracle loss, indicating potential for our scheme.

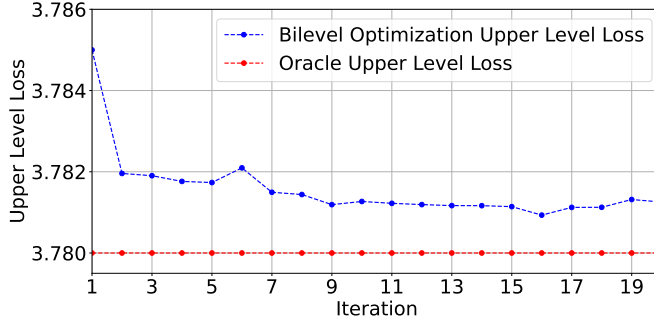


Fig. 11: Upper-level loss in the bilevel optimization formulation (7) plotted over the iterations (after network update step) of the LONDN-MRI scheme at 4x undersampling. We used MoDL with a UNet denoiser and $k = 30$ for neighbor search. In addition, the red line shows an oracle upper-level loss computed using the ground truth test image and its k nearest neighbors.

Effect of Number of Nearest Neighbors on Image Quality: Again, we investigate how the LONDN-MRI algorithm behaves when the number of nearest neighbors is varied to see how it affects the effectiveness of the reconstruction. To test our method, we selected from 10 to 1000 images for the closest neighbors (with NCC metric). The average test reconstruction PSNR for different cases is shown in Fig. 12. Too few local neighbors can make the method prone to overfitting and too many neighbors lead to a lack of scan-specificity and worse performance. 30-50 neighbors provide similar performances.

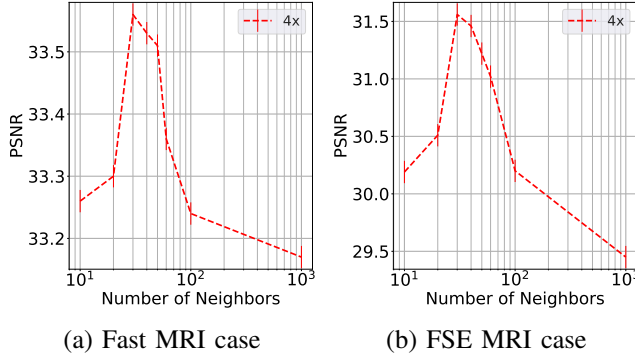


Fig. 12: Average reconstruction PSNR on the fastMRI and FSE MRI test set at 4x undersampling for different numbers of nearest neighbors.

Time Consumption Trade-offs: To further understand the time efficiency of our method across different neighborhood

sizes for practical applicability, we conducted comparative analyses using three models: an image-domain UNet denoiser, MoDL with UNet denoiser, and the MoDL with DIDN denoiser. The experiments were run on an NVIDIA GeForce RTX A5000 GPU. The PSNR vs. runtime trade-offs depicted in Figure 13 shed light on the time consumption for each model configuration. It is observed that some decrease in the number of neighbors leads to reduced time consumption without significantly compromising image quality. In addition, the results show the effectiveness of starting with a pre-trained DIDN model to improve the reconstruction, as it enhances the efficiency of the reconstruction process, reducing it to order of seconds.

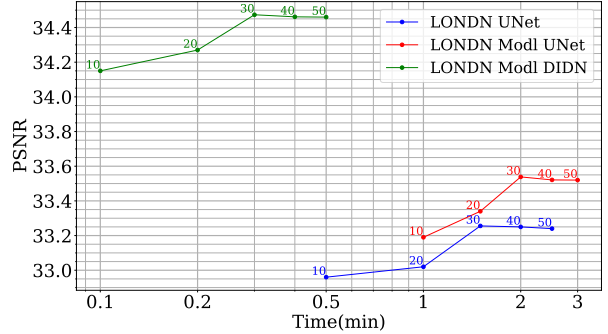


Fig. 13: PSNR vs. runtime trade-offs of various LONDN-MRI models for the fastMRI knee dataset at 4x k-space undersampling. The models include MoDL networks with UNet or DIDN denoisers, as well as a standalone image-domain UNet. The performance was evaluated across different neighbor sizes, which are shown next to each data point. The processing time for these models ranged from 6 seconds to 3 minutes, depending on the neighbor size. Unrolled networks provided better image quality than the UNet denoiser.

D. Generalizability of LONDN-MRI

Here, we present a series of studies to evaluate the generalizability of LONDN-MRI in diverse testing settings.

Performance in the Presence of Planted Features: To assess the capability of LONDN-MRI for accurately reproducing image attributes not found in the training set (a common scenario when detecting pathologies, etc.), we embedded artificial features into a knee image from the fastMRI dataset, drawing inspiration from recent work [46]. We performed 4x undersampling in k-space and reconstructed with the MoDL network (with UNet denoiser) that was trained using 3000 images. In Fig. 15, we observe that LONDN-MRI produces sharper reconstruction of image features and better PSNR compared to the globally trained network. The details or edges of the planted features are better preserved in LONDN-MRI. Moreover, LONDN-MRI provides similar image quality with and without the planted features (Fig. 5), whereas, the globally trained network degrades significantly. This indicates the relatively improved stability and generalizability of the proposed method.

Performance on Data with Lesions: While the previous experiment allowed comparing reconstruction quality with or

without planted features, here we test our method on MRI scans with lesions, which are often regions of abnormal or diseased tissue. We utilize the annotated fastMRI+ data⁶ to evaluate our method’s image reconstruction capabilities, and compare its outcomes with established baselines. For the training phase, the non-lesion dataset was employed for the global training approach with 3000 images whereas LONDN-MRI used 30 adaptively selected images for training (searched from 3000 images). In contrast, during the testing phase, we used 20 scans with lesions. The results, as displayed in Table V, indicate that our method achieves substantially higher PSNR values in comparison to the globally trained baseline as well as the LORAKI method. Furthermore, visualizations in Figure 16 clearly demonstrate the superiority of our method, particularly in the nonspecific white matter lesion areas. Thus, both in terms of visual assessment and PSNR values, our approach outperforms the existing baselines and aligns more closely with the ground truth.

Acceleration	Global	LONDN-MRI (1 iteration)	LONDN-MRI (2 iterations)	Oracle	LORAKI
4x	34.37	34.89	35.1	35.21	32.89
8x	32.05	32.65	32.72	32.77	30.89

TABLE V: Average reconstruction PSNR values (in dB) for the lesion fastMRI+ test set at 4x and 8x k-space undersampling. LONDN-MRI and the global model were trained on the non-lesion dataset.

Performance without Well-Matched Neighbors: Another natural question is how sensitive is the proposed method to using a ‘well matched’ (to the test scan) subset of images in the global training set. One might consider this restrictive. To better evaluate the working of LONDN-MRI, we switched its training with the UNet denoiser from using the 30 closest neighbors to using the 31st to the 60th closest (or less similar) neighbors. Fig. 20 shows an example with the different near-neighbors that are chosen from the 3000 image global training set, ranked based on NCC distance. While the nearest neighbors look quite similar to the test image, the farther ones could be relatively dissimilar in practice. In this case, LONDN-MRI (with 1 iteration) using the 31st to the 60th closest neighbors still reconstructs the test scans well with an average PSNR of 33.34 dB (at 4x k-space undersampling and 15 test images), which is only slightly worse than when using the 30 closest neighbors (33.46 dB). This indicates the proposed approach may not be very sensitive to availability of highly visually matched training data. Indeed, the Stanford FSE data has more variability than fastMRI and our approach performs well on that dataset.

Evaluating Generalization with Limited Training Sets: To facilitate a fairer comparison with scan-adaptive methods such as DIP, LORAKI and RAKI, we conduct experiments utilizing much smaller subsets of the original fastMRI knee dataset, from which the neighbors in LONDN-MRI are selected. We randomly selected 5 to 100 slices for the overall training set in LONDN-MRI. These were chosen from a small random set

of volumes/patients. The goal is to emulate comparisons with DIP, LORAKI, and RAKI when LONDN-MRI operates in a very limited dataset regime. For each overall training set size, we selected the top k similar neighbors at testing time, where k is adjusted based on the dataset size. For example, for a dataset with 5 slices, we selected the top 3 similar scans at test time, and for a dataset with 100 samples, we selected the top 10 neighbors in the search.

The average reconstruction PSNR for the testing scans, plotted in Fig.14, reveals that although there is some decline in performance with decreasing dataset size, the results still surpass those achieved by DIP, RAKI and LORAKI, indicating potential for LONDN-MRI with very limited training sets. While DIP, RAKI and LORAKI adapt purely to the individual test scans without supervision, the LONDN-MRI approach wouldn’t make sense in the 0-paired data regime. In future work, we plan to study hybrid methods leveraging both LONDN-MRI and DIP, i.e., adapting the network based on both similar paired data and the current test scan’s measurements (as in DIP).

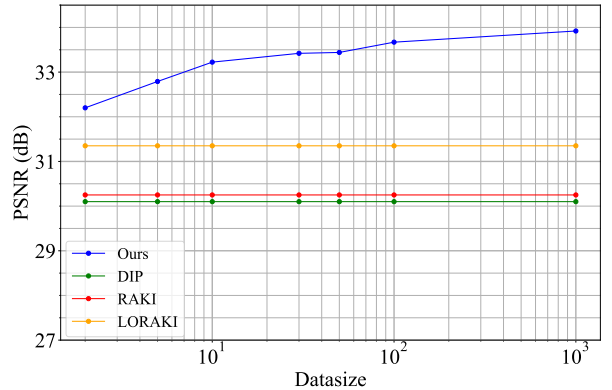


Fig. 14: Average PSNR on test set (from fastMRI) for LONDN-MRI (MoDL network with UNet denoiser) at 4x k-space undersampling for various dataset sizes. Subsets of the dataset are chosen as neighbors in LONDN-MRI at test time. The average PSNR values with DIP, LORAKI, and RAKI, which require no training data are shown as horizontal lines.

Effect of Varying Scan Settings at Test Time: Since the reconstruction network in LONDN-MRI is trained for each scan, we would like to understand better the benefits this provides in terms of letting the network adapt to distinct scan settings. So we chose the MoDL reconstructor with UNet denoiser (with same hyperparameters for training as before) and trained it on the 3000 image set in two ways: with a fixed sampling mask across the images (the mask was padded with zeros to account for slight variations in matrix sizes), and with a different random sampling mask for each image. The first setting was used in previous subsections. For LONDN-MRI, here, we used a different random sampling mask for each test scan, but the network was adapted locally with the same mask used across each (small) local training set. Table VI shows the average PSNR values on the test set with these different strategies as well as with the oracle LONDN-MRI scheme. It is clear that the globally learned model with a fixed sampling

⁶<https://github.com/microsoft/fastmri-plus/tree/main>

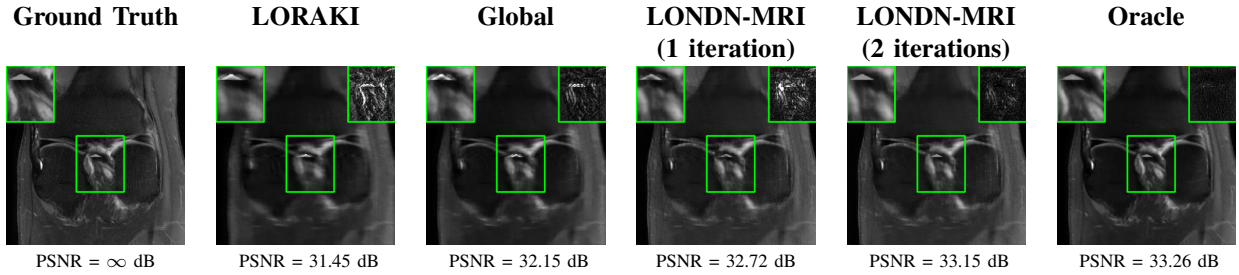


Fig. 15: Visualization of ground truth and reconstructed images using different methods at 4x k-space undersampling. The central portion (with the planted feature) and its reconstruction error map are shown in the top panels in the images.

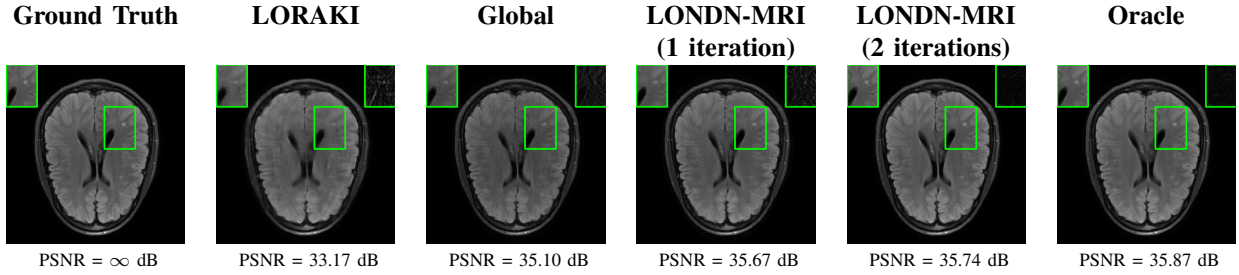


Fig. 16: Visualization of ground truth and reconstructed images using different methods at 4x k-space undersampling for an annotated image from the fastMRI+ dataset, where the interest area is a nonspecific white matter lesion (in green box).

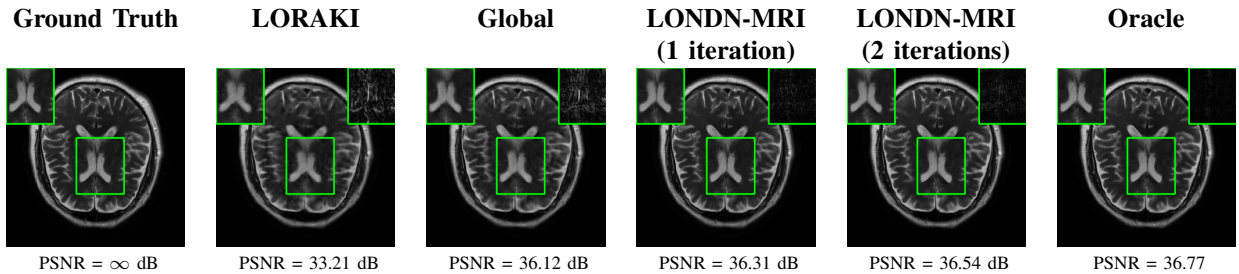


Fig. 17: Visualization of ground-truth and reconstructed images using different methods at 4x k-space undersampling for a T2 contrast MRI scan (with training on T1 contrast scans). A region of interest (in green box) and its error map are also shown.

mask struggles to generalize to the different scan settings at test time. But training the global model with random sampling masks leads to improved reconstruction PSNRs. Importantly, the LONDN-MRI schemes that adapt the reconstruction model to the settings as well as the data for each scan provide marked improvements over both globally learned network settings.

Acceleration	Global Model trained with a fixed mask	Global Model trained with rand. masks	LONDN-MRI (2 iterations)	Oracle LONDN
4x	33.03	33.19	33.56	33.64
8x	30.62	30.84	31.14	31.22

TABLE VI: Average reconstruction PSNR values (in dB) on the test set at 4x and 8x undersampling. The LONDN-MRI results are compared to training a global model with a fixed sampling mask or with random masks.

Results with Different Contrasts: To delve deeper into clinical applicability of our method, we conducted further tests to ascertain its adaptability to different contrasts or weightings

in scans. Conventional deep learning reconstruction techniques may need consistency in contrast between training and testing to achieve optimal results and could struggle with generalization across varied experimental settings. Our method, being scan-specific, could offer some flexibility because of adaptivity to features in test scans. To further study this, we conducted a test, where the global model was trained exclusively on T1 MRI data at 4x and 8x undersampling using 3000 training scans. Subsequent testing was done on T2 contrast MRI data with 20 images. For LONDN-MRI, we used 30 images for local training (searched from 3000 images) for each test scan. The results, presented as box plots in Fig. 18 and visualized with one example in Fig 17, highlight our method’s reconstruction performance in comparison to the globally trained MoDL network and the scan-specific LORAKI scheme. Our method exhibits notable better performance, underscoring its effectiveness in diverse imaging contexts.

Performance with Different Signal-to-Noise Ratios: To assess the performance of LONDN-MRI when the training and tested data have different signal-to-noise ratios (SNRs),

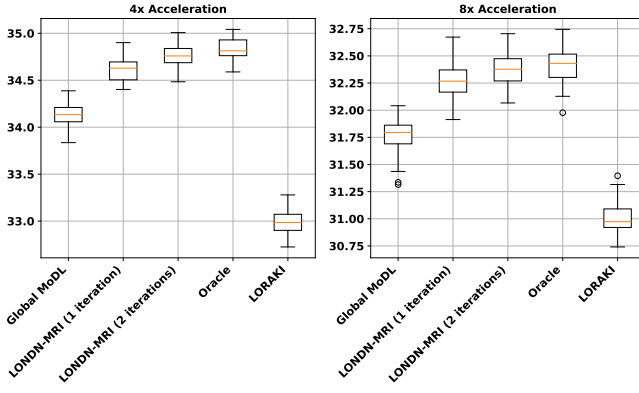


Fig. 18: Box plots for average reconstruction PSNR values (in dB) for different methods for the T2 fastMRI brain test set at 4x and 8x undersampling. LONDN-MRI (trained on T1 contrast fastMRI dataset) results are compared to a model trained globally (on 3000 T1 contrast scans) and to LORAKI.

we conducted tests on scans from the fastMRI knee dataset that were subjected to additive random Gaussian noise with a variance of 0.01 for the real and imaginary parts of the noise. The globally and locally trained models at 4x and 8x undersampling used data without added noise, and the training settings were the same as before in Section IV-A. Our findings revealed a general decline in reconstruction performance across all methods, attributable to the different SNRs between training and testing. Despite this, LONDN-MRI displays better capability in handling noise perturbations, with a wider performance gap over the globally trained model. This is clear from the PSNR values depicted in the corresponding box plots in Fig. 19.

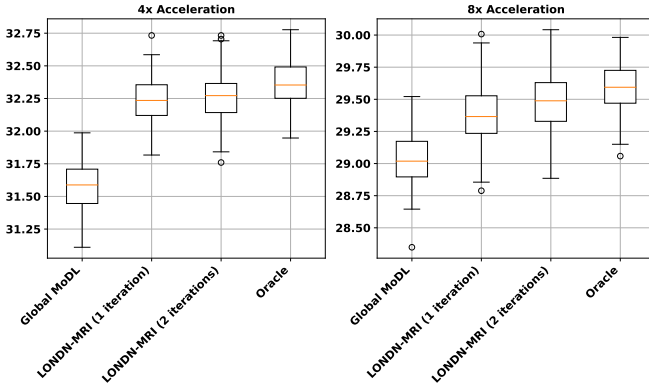


Fig. 19: Box plots of average reconstruction PSNR values (in dB) for different methods on the fastMRI knee test set at 4x and 8x undersampling. For the test dataset, we added zero-mean Gaussian noise to the measurements with standard deviation $\sigma = 0.01$ for the real and imaginary parts of the noise. All training data used did not include additional noise.

V. DISCUSSION

We proposed a novel LONDN-MRI reconstruction technique that efficiently matches test reconstructions to a cluster

of a dataset, where networks are adaptively estimated on images most related to a current scan. Our results on the multi-coil fastMRI brain and knee datasets, fastMRI+, and the Stanford FSE dataset showed promise for our patient-adaptive network estimation scheme. The approach does not require pre-training and can thus readily handle changes in the training set. Additionally, the networks in LONDN-MRI can be randomly initialized and trained adaptively on very small datasets, and such networks outperformed models trained globally on much larger datasets (with lengthy training times). For example, for fastMRI knee scans, LONDN-MRI with 2 alternations involving MoDL with a randomly initialized UNet denoiser took 5 minutes to run on a NVIDIA GeForce RTX A5000 GPU (with batchsize of 6 and 200 epochs each time to update networks locally). While LONDN-MRI outperformed the scan-adaptive methods such as DIP, RAKI, and LORAKI in image quality, the runtimes for the methods were somewhat similar. DIP takes about 5 minutes to reach peak performance (over iterations) with the same GPU, while RAKI and LORAKI took 3 mins and 4 mins, respectively. LONDN-MRI requires only a few images (e.g., 30) to train networks, with often 200-250 epochs for locally updating randomly initialized networks such as the UNet. Fewer epochs (often 10 suffices) of update were needed with pre-trained networks such as the pre-trained DIDN, resulting in runtimes of only 18 seconds per iteration of LONDN-MRI (Fig. 13). Of course, a globally trained model would run faster at inference time. For example, MoDL with pre-trained DIDN denoiser takes 8 seconds on average to reconstruct fastMRI knee images. Note that the neighbor search process in the proposed method is highly efficient. We find 20-30 images from 3000 images to train the model in about 10 seconds, while the overall algorithm takes minutes. The neighbor search is also highly parallelizable.

When compared to the supervised global model, the proposed method offers consistently improved reconstruction quality in terms of PSNR, SSIM, and HFEN metrics. Additionally, we demonstrated that the local model adapts better to test time changes (such as changes to the sampling mask, scan contrast, SNR, presence of anomalies, etc.) compared to a globally learned (and fixed) model. Our approach produced marked improvements for the Stanford FSE dataset, and noticeable improvements for fastMRI/fastMRI+. Additionally, our study with different distance metrics revealed they have only slight effect on reconstruction quality. The NCC metric provided the best reconstruction quality and was thus used in our studies. We conjecture that a learned distance metric [48] could further enhance the performance of LONDN-MRI.

VI. CONCLUSIONS

This paper examined supervised learning of deep unrolled networks at reconstruction time for MRI by exploiting training sets along with local modeling and clustering. We showed advantages for this approach at different k-space undersampling factors over networks learned in a global manner on larger data sets. The training may be connected to a bilevel optimization problem. We also compared different distance metrics for finding neighbors in our approach and regularization to reduce

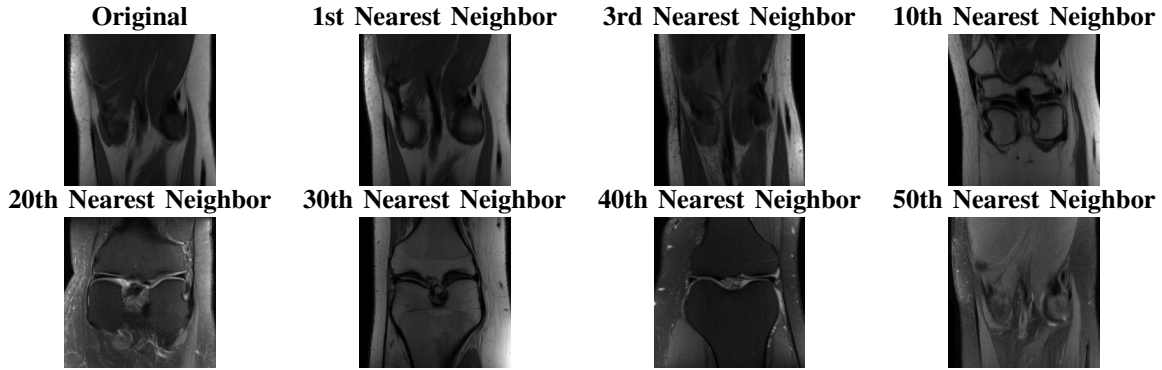


Fig. 20: An image is shown along with different nearest neighbors from the fastMRI dataset.

local overfitting. We intend to expand our studies in the future by incorporating non-Cartesian undersampling patterns, such as radial and spiral patterns, as well as deploying them to 3D settings and other imaging modalities. Additionally, the method’s generalizability will be further examined, with a particular emphasis on heterogeneous datasets. To handle more extreme training-test data variations such as unseen anatomies, we plan to explore patch-based neighbors in local learning schemes for future work. We showed benefits for both randomly seeded training of simple models and for fine tuning of sophisticated pre-trained models, and believe our methodology could be applied to a variety of deep learning-based tasks (even beyond image reconstruction) effectively to improve overall performance. Finally, metric learning [48] to improve local clustering and subsequent network adaptation will be an important future direction.

REFERENCES

- [1] I. A. Elbakri and J. A. Fessler, “Statistical image reconstruction for polyanergetic X-ray computed tomography,” *IEEE Transactions on Medical Imaging*, vol. 21, no. 2, pp. 89–99, 2002.
- [2] J. A. Fessler, “Model-Based Image Reconstruction for MRI,” *IEEE Signal Processing Magazine*, vol. 27, no. 4, pp. 81–89, 2010.
- [3] D.L. Donoho, “Compressed sensing,” *IEEE Transactions on Information Theory*, vol. 52, no. 4, pp. 1289–1306, 2006.
- [4] M. Kivanc Mihcak, I. Kozintsev, K. Ramchandran, and P. Moulin, “Low-complexity image denoising based on statistical modeling of wavelet coefficients,” *IEEE Signal Processing Letters*, vol. 6, no. 12, pp. 300–303, 1999.
- [5] S. Ma, W. Yin, Y. Zhang, and A. Chakraborty, “An efficient algorithm for compressed MR imaging using total variation and wavelets,” in *2008 IEEE Conference on Computer Vision and Pattern Recognition*, 2008, pp. 1–8.
- [6] S. Ravishankar and Y. Bresler, “MR image reconstruction from highly undersampled k-space data by dictionary learning,” *IEEE Transactions on Medical Imaging*, vol. 30, no. 5, pp. 1028–1041, 2011.
- [7] S. G. Lingala and M. Jacob, “Blind compressive sensing dynamic MRI,” *IEEE Transactions on Medical Imaging*, vol. 32, no. 6, pp. 1132–1145, 2013.
- [8] S. Ravishankar, R. R. Nadakuditi, and J. A. Fessler, “Efficient sum of outer products dictionary learning (SOUP-DIL) and its application to inverse problems,” *IEEE Transactions on Computational Imaging*, vol. 3, no. 4, pp. 694–709, 2017.
- [9] Q. Xu, H. Yu, X. Mou, L. Zhang, J. Hsieh, and G. Wang, “Low-dose x-ray ct reconstruction via dictionary learning,” *IEEE Transactions on Medical Imaging*, vol. 31, no. 9, pp. 1682–1697, 2012.
- [10] S. Ye, Z. Li, M. T. McCann, Y. Long, and S. Ravishankar, “Unified Supervised-Unsupervised (SUPER) Learning for X-Ray CT Image Reconstruction,” *IEEE Transactions on Medical Imaging*, vol. 40, no. 11, pp. 2986–3001, 2021.
- [11] S. Ravishankar and Y. Bresler, “Learning sparsifying transforms,” *IEEE Transactions on Signal Processing*, vol. 61, no. 5, pp. 1072–1086, 2012.
- [12] S. Ravishankar, J. C. Ye, and J. A. Fessler, “Image reconstruction: From sparsity to data-adaptive methods and machine learning,” *Proceedings of the IEEE*, vol. 108, no. 1, pp. 86–109, 2019.
- [13] B. Wen, S. Ravishankar, L. Pfister, and Y. Bresler, “Transform learning for magnetic resonance image reconstruction: From model-based learning to building neural networks,” *IEEE Signal Processing Magazine*, vol. 37, no. 1, pp. 41–53, 2020.
- [14] A. Ghosh, M. T. McCann, and S. Ravishankar, “Bilevel learning of l_1 -regularizers with closed-form gradients (blorc),” *arXiv preprint arXiv:2111.10858*, 2021.
- [15] O. Ronneberger, P. Fischer, and T. Brox, “U-net: Convolutional networks for biomedical image segmentation,” in *Medical Image Computing and Computer-Assisted Intervention – MICCAI 2015*, 2015, pp. 234–241.
- [16] K. H. Jin, M. T. McCann, E. Froustey, and M. Unser, “Deep convolutional neural network for inverse problems in imaging,” *IEEE Trans. Im. Proc.*, vol. 26, no. 9, pp. 4509–22, Sept. 2017.
- [17] C. Feng, Y. Yan, H. Fu, L. Chen, and Y. Xu, “Task Transformer Network for Joint MRI Reconstruction and Super-Resolution,” in *International Conference on Medical Image Computing and Computer Assisted Intervention (MICCAI)*, 2021.
- [18] K. Lei, M. Mardani, J. M. Pauly, and S. Vasanawala, “Wasserstein GANs for MR Imaging: From Paired to Unpaired Training,” *IEEE Transactions on Medical Imaging*, vol. 40, no. 1, pp. 105–115, Jan 2021.
- [19] S. U. H. Dar, M. Özbeý, A. B. Çatlı, and T. Çukur, “A transfer-learning approach for accelerated MRI using deep neural networks,” *Magnetic resonance in medicine*, vol. 84, no. 2, pp. 663–685, 2020.
- [20] H. K. Aggarwal, M. P. Mani, and M. Jacob, “MoDL: model-based deep learning architecture for inverse problems,” *IEEE Trans. Med. Imaging*, vol. 38, no. 2, pp. 394–405, 2019.
- [21] H. Zheng, F. Fang, and G. Zhang, “Cascaded dilated dense network with two-step data consistency for MRI reconstruction,” *Advances in Neural Information Processing Systems*, vol. 32, 2019.
- [22] J. Schlemper, J. Caballero, J. V. Hajnal, A. Price, and D. Rueckert, “A Deep Cascade of Convolutional Neural Networks for Dynamic MR Image Reconstruction,” *IEEE Transactions on Medical Imaging*, vol. 37, no. 2, pp. 491–503, 2018.
- [23] Y. Yang, J. Sun, H. Li, and Z. Xu, “Deep ADMM-Net for compressive sensing MRI,” in *Advances in Neural Information Processing Systems*, 2016, pp. 10–18.
- [24] K. Hammernik, T. Klatzer, E. Kobler, M. P. Recht, D. K. Sodickson, Thomas Pock, and Florian Knoll, “Learning a variational network for reconstruction of accelerated MRI data,” *Magnetic resonance in medicine*, vol. 79, no. 6, pp. 3055–3071, 2018.
- [25] Y. Romano, M. Elad, and P. Milanfar, “The Little Engine That Could: Regularization by Denoising (RED),” *SIAM Journal on Imaging Sciences*, vol. 10, no. 4, pp. 1804–1844, 2017.
- [26] G. T. Buzzard, S. H. Chan, S. Sreehari, and C. A. Bouman, “Plug-and-play unplugged: optimization-free reconstruction using consensus equilibrium,” *SIAM J. Imaging Sci.*, vol. 11, no. 3, pp. 2001–20, Jan. 2018.
- [27] J. Zhang and B. Ghanem, “ISTA-Net: Interpretable optimization-inspired deep network for image compressive sensing,” in *Proceedings of the IEEE conference on Computer Vision and Pattern Recognition*, 2018, pp. 1828–1837.

- [28] Z Wang, C Qian, D Guo, H Sun, R Li, B Zhao, and X Qu, “One-dimensional deep low-rank and sparse network for accelerated MRI,” *IEEE Transactions on Medical Imaging*, vol. 42, no. 1, pp. 79–90, 2023.
- [29] V. Antun, F. Renna, C. Poon, B. Adcock, and A. C. Hansen., “On instabilities of deep learning in image reconstruction and the potential costs of AI,” *Proceedings of the National Academy of Sciences*, vol. 117, no. 48, pp. 30088–30095, May 2020.
- [30] C. Chen, Y. Liu, P. Schniter, M. Tong, K. Zareba, O. Simonetti, L. Potter, and R. Ahmad, “Ocmr (v1.0)—open-access multi-coil k-space dataset for cardiovascular magnetic resonance imaging,” *arXiv preprint arXiv:2008.03410*, 2020.
- [31] J. Zbontar et al, “fastMRI: An Open Dataset and Benchmarks for Accelerated MRI,” <https://fastmri.med.nyu.edu/>, 2019, arXiv preprint arXiv:1811.08839.
- [32] D. Ulyanov, A. Vedaldi, and V. Lempitsky, “Deep image prior,” in *Proceedings of the IEEE Conference on Computer Vision and Pattern Recognition*, 2018, pp. 9446–9454.
- [33] M. Z. Darestani and R. Heckel, “Accelerated MRI with un-trained neural networks,” *IEEE Transactions on Computational Imaging*, vol. 7, pp. 724–733, 2021.
- [34] M. Akçakaya, S. Moeller, S. Weingärtner, and K. Uğurbil, “Scan-specific Robust Artificial-neural-networks for k-space Interpolation (RAKI) Reconstruction: Database-free Deep Learning for Fast Imaging,” *Magnetic Resonance in Medicine*, vol. 81, no. 2, pp. 439–453, 2019.
- [35] A. Deshmane, V. Gulani, M. A. Griswold, and N. Seiberlich, “Parallel MR imaging,” *Journal of Magnetic Resonance Imaging*, vol. 36, no. 1, pp. 55–72, 2012.
- [36] T. H. Kim, P. Garg, and J. P. Haldar, “Loraki: Autocalibrated recurrent neural networks for autoregressive MRI reconstruction in k-space,” *arXiv preprint arXiv:1904.09390*, 2019.
- [37] R. A. Lobos, A. Javed, K. S. Nayak, W.S. Hoge, and J. P. Haldar, “Robust autocalibrated loraks for epi ghost correction,” *IEEE International Symposium on Biomedical Imaging*, vol. 36, no. 1, pp. 663–666, 2018.
- [38] B. Yaman, S. A. H. Hosseini, S. Moeller, J. Ellermann, K. Ugurbil, and M. Akçakay, “Self-supervised learning of physics-guided reconstruction neural networks without fully sampled reference data,” *Magnetic Resonance in Medicine*, vol. 84, no. 6, pp. 3172–3191, 2020.
- [39] A. Lahiri, S. Ravishankar, and J. A. Fessler, “Combining supervised and semi-blind dictionary (Super-BReD) learning for MRI reconstruction,” in *Proc. Intl. Soc. Mag. Res. Med.*, 2020, p. 3456.
- [40] M. Lustig, D. Donoho, and J. M. Pauly, “Sparse MRI: The application of compressed sensing for rapid MR imaging,” *Magnetic Resonance in Medicine: An Official Journal of the International Society for Magnetic Resonance in Medicine*, vol. 58, no. 6, pp. 1182–1195, 2007.
- [41] C. Crockett and J. A. Fessler, “Bilevel methods for image reconstruction,” *arXiv preprint arXiv:2109.09610*, 2021.
- [42] F. Knoll et al, “fastMRI: A Publicly Available Raw k-Space and DICOM Dataset of Knee Images for Accelerated MR Image Reconstruction Using Machine Learning,” *Radiology: Artificial Intelligence*, vol. 2, no. 1, pp. e190007, 2020, <https://fastmri.med.nyu.edu/>.
- [43] J. Y. Cheng, “Stanford 2D FSE,” <http://mridata.org/list?project=Stanford2DFSE>, June 2019, Accessed: Mar. 2024.
- [44] M. Uecker, “mrirecon/bart: version 0.4.03,” <https://github.com/mrirecon/bart>, Apr. 2018.
- [45] S. Yu, B. Park, and J. Jeong, “Deep Iterative Down-Up CNN for Image Denoising,” in *2019 IEEE/CVF Conference on Computer Vision and Pattern Recognition Workshops (CVPRW)*, 2019, pp. 2095–2103.
- [46] A. Lahiri, G. Wang, S. Ravishankar, and J. A. Fessler, “Blind Primed Supervised (BLIPS) Learning for MR Image Reconstruction,” *IEEE Transactions on Medical Imaging*, vol. 40, no. 11, pp. 3113–3124, 2021.
- [47] Z. Wang, A. C. Bovik, H. R. Sheikh, and P. E. Simoncelli, “Image quality assessment: From error visibility to structural similarity,” *IEEE Trans. Image Process.*, vol. 13, no. 4, pp. 600–612, 2004.
- [48] M Kaya and H .S Bilge, “Deep metric learning: A survey,” *Symmetry*, vol. 11, no. 9, pp. 1066, 2019.